Clim Dyn
DOI 10.1007/s00382-016-3306-1

Southern European rainfall reshapes the early-summer circumglobal teleconnection after the late 1970s

Zhongda Lin[1] · Fei Liu[2] · Bin Wang[2,3] · Riyu Lu[1] · Xia Qu[1]

Received: 30 December 2015 / Accepted: 28 July 2016

Abstract The summer circumglobal teleconnection (CGT), which crucially affects mid-latitude climate in the Northern Hemisphere, is generally characterized by a mid-latitude wave train along the strong upper-tropospheric westerly jet. In this study a significant change is identified in the spatial pattern of the early-summer CGT after the late 1970s: An additional high-latitude wave train has occurred over northern Eurasia. Based on observational evidences and simulation results with a linear baroclinic model, it is proposed that the post-1970s CGT change is induced by enhanced impact of rainfall over southern Europe (SE) after the late 1970s. Specifically, the mid-latitude wave train of CGT in early summer is dominated by Indian rainfall before the late 1970s but by both rainfall over India and SE after the late 1970s; the high-latitude wave train of CGT occurring after the late 1970s, however, is induced only by the SE rainfall. The coupled Indian and SE rainfall after the late 1970s, which is probably due to the basic flow change over the North Atlantic, induce both mid-latitude and high-latitude wave trains of the CGT.

✉ Zhongda Lin
zdlin@mail.iap.ac.cn

[1] State Key Laboratory of Numerical Modelling for Atmospheric Sciences and Geophysical Fluid Dynamics, Institute of Atmospheric Physics, Chinese Academy of Sciences, Beijing 100029, China

[2] Earth System Modeling Center and Climate Dynamics Research Center, Nanjing University of Information Science and Technology, Nanjing 210044, Jiangsu, China

[3] Department of Atmospheric Sciences and Atmosphere–Ocean Research Center, University of Hawai'i at Mānoa, Honolulu, HI 96822, USA

Keywords Circumglobal teleconnection · Southern European summer rainfall · Indian rainfall · Decadal change · North Atlantic westerly jet

1 Introduction

The summertime circumglobal teleconnection (CGT) is characterized by a wave train in mid latitudes of the Northern Hemisphere along the upper-tropospheric westerly jet (Ding and Wang 2005). Portions of CGT were also referred to as the "Silk Road" pattern over Eurasian continent (Lu et al. 2002; Enomoto et al. 2003; Enomoto 2004) and the "Tokyo-Chicago express" over the East Asia–North Pacific–North America region (Wang et al. 2001; Lau and Weng 2002). Previous studies have found that the CGT significantly affects mid-latitude climate in the Northern Hemisphere (Ding and Wang 2005; Sun et al. 2008; Li et al. 2010; Huang et al. 2011; Saeed et al. 2011a; Schubert et al. 2011; Soon et al. 2011; Sun and Wang 2012; Lin 2014; Huang et al. 2015).

Many studies were, therefore, devoted to understanding the mechanisms for formation and maintenance of the CGT. The CGT can be explained, physically, as an eastward-propagating Rossby wave train trapped within the upper-tropospheric westerly jet, due to the waveguide effect of the strong westerly (Hoskins and Ambrizzi 1993; Ambrizzi et al. 1995). It is significantly affected by tropical monsoon heat forcing (Ding and Wang 2005; Yasui and Watanabe 2010; Ding et al. 2011; Yim et al. 2014), though it could also extract barotropic kinetic energy (Sato and Takahashi 2006; Kosaka et al. 2009; Ding et al. 2011) and available potential energy through baroclinic energy conversion (Kosaka et al. 2009; Chen et al. 2013) from the basic flow. Some studies have highlighted the role of the

Published online: 05 August 2016

Indian summer monsoon rainfall (Ding and Wang 2005; Lin 2009; Saeed et al. 2011b; Liu and Wang 2013). The Indian heat forcing can trigger a westward-propagating Gill-type Rossby wave response and form an anticyclonic anomaly in the entrance of the Asian westerly jet in the upper troposphere (Rodwell and Hoskins 1996), initiating an eastward-propagating CGT-like wave train trapped in the strong westerly jet (Enomoto et al. 2003). Similarly, the anticyclonic disturbance over the eastern Mediterranean region can also be excited by the divergent flow–induced vorticity advection, due to the heat forcing over the tropical western Indian Ocean (Chen and Huang 2012). Additionally, the CGT is also contributed to by diabatic heat forcings over the monsoon regions of North America (Yasui and Watanabe 2010) and northern Africa (Yim et al. 2014).

The mid-latitude diabatic heating also feeds back to the variation of the CGT (Yasui and Watanabe 2010). Yasui and Watanabe (2010) investigated thermodynamical forcings of the CGT in a dry atmospheric general circulation model. They proposed that the mid-latitude diabatic heat forcing around the Mediterranean Sea region, rather than those over tropical monsoon regions, can form the CGT pattern most efficiently. Recently, Lin and Lu (2016) found that the summer rainfall over southern-central Europe can also trigger a downward CGT-like wave train in mid latitudes of the Northern Hemisphere.

In addition to the interannual variations, the CGT also exhibit an interdecadal change in its intensity after the late 1970s (Wang et al. 2012). During the recent epoch after the late 1970s, the major centers related to the CGT weakened over the North Atlantic–Europe sector. The weakening of the CGT is resulted from the decreased interannual variability of the Indian summer monsoon rainfall due to the change of the ENSO properties. The reduced interannual variability weakens its connection with the mid-latitude circulations and then the intensity of the CGT.

In the present study, the authors reveal that in addition to the weakened intensity of the summer-mean CGT, the spatial pattern of the CGT in early summer also experienced a significant change over Eurasian continent around the late 1970s. Two wave trains are identified related to the CGT after the late 1970s: one in mid latitudes along the upper-tropospheric Asian westerly jet, resembling that before the late 1970s, and the other in high latitudes over northern Eurasia. It is proposed that the post-1970s CGT pattern change is attributed to the enhanced effect of the early-summer rainfall over southern Europe (SE) after the late 1970s.

The structure of the remainder is organized as follows. Section 2 introduces data and a linear baroclinic model (LBM) used in this study. Change in the spatial pattern of the early-summer CGT is illustrated in Sect. 3. The role of rainfall over SE on the CGT pattern change is investigated in Sect. 4. Similarly, features of the CGT in July and August are explored in Sect. 5. Section 6 presents conclusion.

2 Data and model

The monthly atmospheric data used in this study come from the European Centre for Medium-Range Weather Forecasts (ECMWF) 40-years Re-Analysis (ERA–40) during 1958–2002 (Uppala et al. 2005). The monthly land precipitation data are from the Climatic Research Unit (CRU), University of East Anglia, UK (Mitchell and Jones 2005). Also used are the National Oceanic and Atmospheric Administration (NOAA)'s global precipitation reconstruction datasets (Chen et al. 2002). The horizontal resolution of precipitation is $0.5° \times 0.5°$ for the CRU data and $2.5° \times 2.5°$ for the NOAA data.

To focus on interannual variations, the long-term trend and decadal variations during the whole ERA-40 period (1958–2002), with periods longer than eight years, are removed using Fourier harmonic analysis method. The Student's t test is used to obtain the statistical significance for the results in this study.

The model used in this study consists of primitive equations linearized about the monthly climatology (Watanabe and Kimoto 2000). The heating patterns associated with the CGT serve as prescribed forcings for the dry version of the linear model. This allows one to investigate the possible roles that the regional heat sources and sinks play in the CGT. The model adopts a horizontal resolution of T42 and vertical 20 levels using the sigma (σ) coordinate system, and includes a horizontal (vertical) diffusion, Rayleigh friction, and Newtonian damping. The horizontal diffusion has a damping timescales of 6 h for the smallest wave, and the Rayleigh friction and Newtonian damping have a time scale of $(0.5\ \text{day})^{-1}$ for $\sigma \geq 0.9$ and $(1\ \text{day})^{-1}$ for $\sigma \leq 0.03$, while $(20\ \text{day})^{-1}$ between them. To obtain the linear atmospheric response to forcing, in this study we adopt a time integration method. The integration is continued up to 20 days, and the results averaged for days 16–20 are shown as the steady response to a prescribed diabatic heat forcing since the circulation response approaches the steady state approximately after day 15, same as the result of Yun et al. (2011).

3 Change in the early-summer CGT around the late 1970s

To investigate the interdecadal change of the CGT pattern around the late 1970s, the whole period (1958–2002) of the ERA–40 reanalysis data were divided into two 22-years epochs: 1958–1979 and 1981–2002. Figure 1 shows the

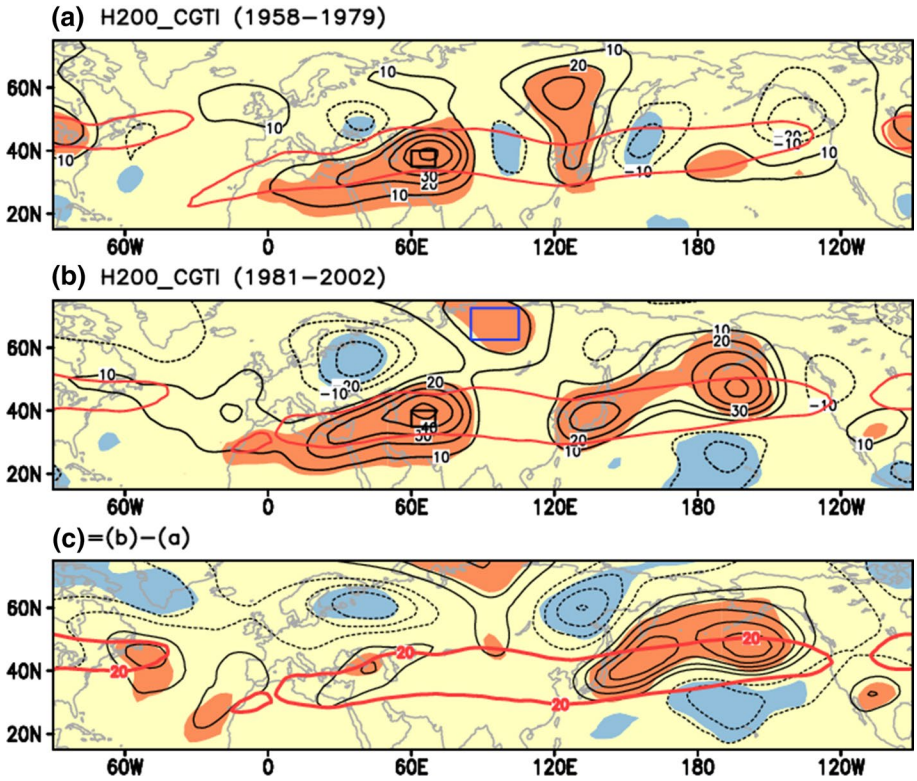

Fig. 1 Anomalies of geopotential height at 200 hPa (H200) regressed against the CGTI in June during **a** 1958–1979, **b** 1981–2002, and **c** their difference. *Shading* indicates significance at the 95 % confidence level and contour interval is 10 gpm. The *red thick contour* depicts the strong westerly jet exceeding 20 m s^{-1} at 200 hPa

positive phase of the early-summer CGT pattern, which is depicted by geopotential height anomalies at 200 hPa (H200) regressed against the CGT index (CGTI) in June during the two epochs, respectively. The CGTI is defined as 200-hPa geopotential height averaged over west-central Asia (35°–40°N, 60°–70°E), in the same manner as Ding and Wang (2005). During the pre-1980 epoch, a wave train along the strong mid-latitude westerly jet in the upper troposphere is identified (Fig. 1a). The mid-latitude wave train, over Eurasian continent, consists of two positive centers over southwest Asia and East Asia and two negative centers over eastern Europe and northwest China. This mid-latitude wave train is also seen during the post-1980 epoch (Fig. 1b), with a spatial pattern similar to that during the pre-1980 epoch. Meanwhile, a notable high-latitude wave train is emanated northeastward from the negative anomaly over eastern Europe to Far East, with a positive anomaly centered over northern central Siberia and a negative anomaly over eastern Siberia. The appearance of the high-latitude wave train after the late 1970s indicates a significant change in the CGT spatial pattern. The CGT pattern change is more clearly illustrated by their difference (Fig. 1c), with a wave-train pattern over northern Eurasia. Also noticed are a positive H200 anomaly over mid-high latitudes of the North Pacific, suggesting a weakened Aleutian low probably due to the enhanced connection of the CGT with the Pacific–North American pattern, and a meridional dipole pattern over the North Atlantic.

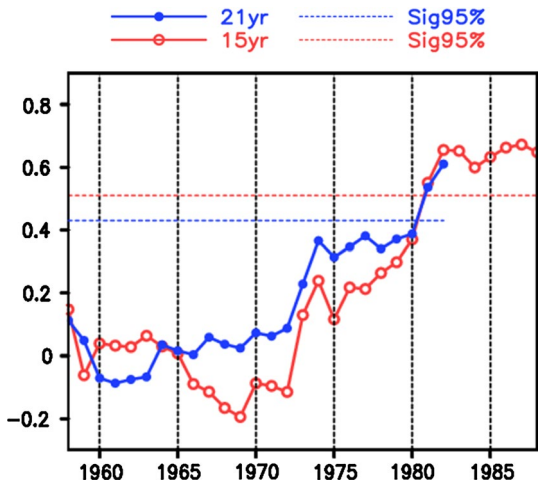

Fig. 2 Sliding correlation coefficient of the CGTI with H200 anomalies in June averaged over the region (62.5°–72.5°N, 85°–105°E), depicted by the *blue box* in Fig. 1b, with a window of 15 years (*red solid line*) and of 21 years (*blue solid line*). *Dashed lines* denote their corresponding significance at the 95 % confidence level. The year in the X-axis represents the 1st year of the sliding window, for example, year 1981 represents the sliding window of 1981–1995 (15 years) and 1981–2001 (21 years)

To better illustrate the interdecadal change of the CGT pattern over northern Eurasia, H200 anomalies over northern central Siberia (62.5°–72.5°N, 85°–105°E), the region with significant anomalies related to the CGTI after the

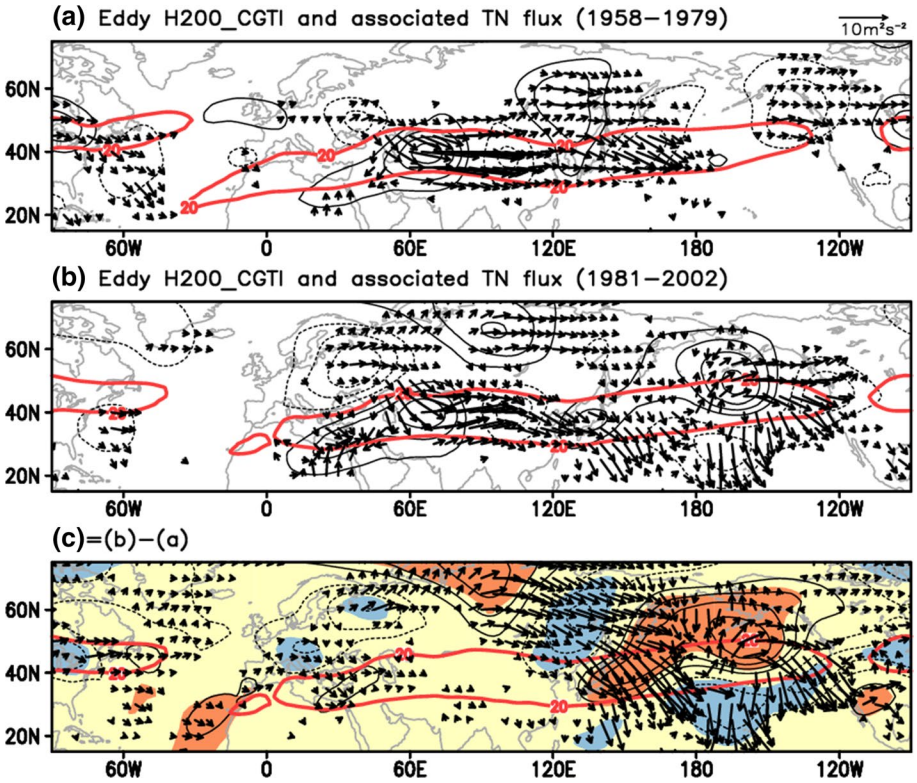

Fig. 3 **a**–**b** Anomalies of eddy H200 (contour with interval of 10 gpm), in which zonal-mean H200 is subtracted, regressed against the CGTI and the associated Takaya and Nakamura wave flux (vector) during **a** 1958–1979, **b** 1981–2002, and **c** their difference. *Red thick contour* depicts the strong westerly jet exceeding 20 m s^{-1} at 200 hPa. *Shading* indicates significance at the 95 % confidence level

late 1970s (Fig. 1b), are averaged to depict the high-latitude wave train. Its sliding correlation with the CGTI is shown in Fig. 2. The correlation, with a sliding window of 21 years, is weak during the 1960s and 1970s, and becomes significant at the 95 % confidence level since 1981. A similar result is obtained based on a sliding window of 15 years. The enhanced correlation confirms our previous result that the CGT pattern had significantly changed, featuring a significant high-latitude wave train over northern Eurasian continent after the late 1970s. It also proves that the division of the two epochs 1958–1979 and 1981–2002 is reasonable and physically consistent with the change of the early-summer CGT pattern. A similar decadal change in the CGT pattern (figure not shown) is also obtained around the late 1970s using the NCEP/NCAR reanalysis data extended back to 1948 (Kalnay et al. 1996). Accordingly, results are presented in the following sections based on the two epochs: the pre-1980 epoch (1958–1979) and the post-1980 epoch (1981–2002) using the ERA–40 data only in this study.

To investigate dynamical characteristic of the stationary Rossby wave trains related to the CGT, the zonal and meridional components of a wave-activity flux for stationary Rossby waves ($\boldsymbol{W}$) are employed following Takaya and Nakamura (2001), which is defined as

$$\boldsymbol{W} = \frac{1}{2|\overline{\boldsymbol{V}}|}\begin{pmatrix} \overline{u}(\psi_x'^2 - \psi'\psi_{xx}') + \overline{v}(\psi_x'\psi_y' - \psi'\psi_{xy}') \\ \overline{u}(\psi_x'\psi_y' - \psi'\psi_{xy}') + \overline{v}(\psi_y'^2 - \psi'\psi_{yy}') \end{pmatrix},$$

where $|\boldsymbol{V}|$ is the magnitude of the horizontal vector wind (u, v) and ψ is the stream function; variables with an overbar represent their climatological mean in June during the pre-1980 epoch (Fig. 3a) and the post-1980 epoch (Fig. 3b); variables with subscript and prime notations signify their partial derivatives and anomalies associated with the CGTI, respectively.

The two-dimensional horizontal wave fluxes at 200 hPa related to the CGT during the pre- and post-1980 epochs are shown in Fig. 3. A zonally-propagating wave flux, originated over eastern Europe, is identified along the Asian westerly jet during the pre-1980 epoch (Fig. 3a). The CGT-related wave flux during the post-1980 epoch (Fig. 3b) is, however, divided into two branches over eastern Europe: one propagates southeastward into the Asian westerly jet and then extends eastward within the westerly jet, the same as that during the pre-1980 epoch (Fig. 3a), and the other diverts northeastward via central Siberia to Far East. The wave flux propagation is consistent with the spatial pattern of the CGT, with a mid-latitude wave train along the subtropical westerly jet during the pre- and post-1980 epochs and an additional high-latitude wave train over northern Eurasia during the post-1980 epoch, suggesting the nature of the stationary Rossby wave propagation for the CGT pattern.

The difference of wave flux shows that the change of the spatial pattern of the CGT over Eurasia after the late 1970s is attributed to the stationary Rossby wave flux

propagation over northern Eurasia from eastern Europe via central Siberia to Far East (Fig. 3c). The high-latitude wave flux diverts over Europe with a weak southeastward propagation of wave flux from SE into the Asian westerly jet. In theory, the mid-latitude wave disturbance can propagate both northeastward and southeastward, decided by the sign of meridional wavenumber of the stationary Rossby wave (Hoskins and Karoly 1981; Hoskins and Ambrizzi 1993). The division of the northeastward and southeastward propagation of the wave flux over Europe (Fig. 3c), concurrent with the origin of the wave flux related to the CGT over eastern Europe during the both epochs (Fig. 3a, b), suggests the early-summer CGT change may arise from Europe. In the next section, possible impact of European forcing on the decadal CGT pattern change is investigated.

4 Relative role of the SE and Indian rainfall in the early-summer CGT pattern change

4.1 Observational evidence

Several previous studies have noticed the relationship between summer rainfall over Europe and the CGT. Saeed et al. (2014) revealed a CGT-like wave train extending from the North Pacific to the Eurasian region, which is responsible for a rainfall dipole pattern between western and eastern Europe in summer. Lin and Lu (2016) found a significant link between the summer-mean rainfall over southern-central Europe and the CGT. They proposed that the southern-central Europe rainfall can trigger a downstream-developed CGT-like wave train with a negative H200 anomaly over eastern Europe and a positive H200 anomaly over west-central Asia, similar to the part of mid-latitude wave train related to the CGTI (Fig. 1). To investigate relationship between European rainfall and the CGT pattern change in early summer, Fig. 4b, c show the CGTI-related CRU rainfall anomalies over European region during the pre- and post-1980 epochs, respectively. In the positive phase of the CGT pattern, rainfall is significantly reduced over SE during the second epoch (Fig. 4c), but not during the first epoch (Fig. 4b). The correlation coefficients of the CGTI with the SE rainfall index (SERI) are −0.53 during 1981–2002, significant at the 95 % confidence level, and only −0.16 during 1958–1979 (Table 1). The two correlation coefficients are significantly different at the 90 % confidence level tested by the Fisher's z-transformation method (Fisher 1921). The SERI is defined as mean rainfall averaged over the SE region (40°–50°N, 0°–30°E) where strong rainfall interannual variability occurs, with standard deviation exceeding 1 mm per day (Fig. 4a). The time series of the SERI are presented in Fig. 5. The same analysis is performed based on the NOAA global precipitation data. A

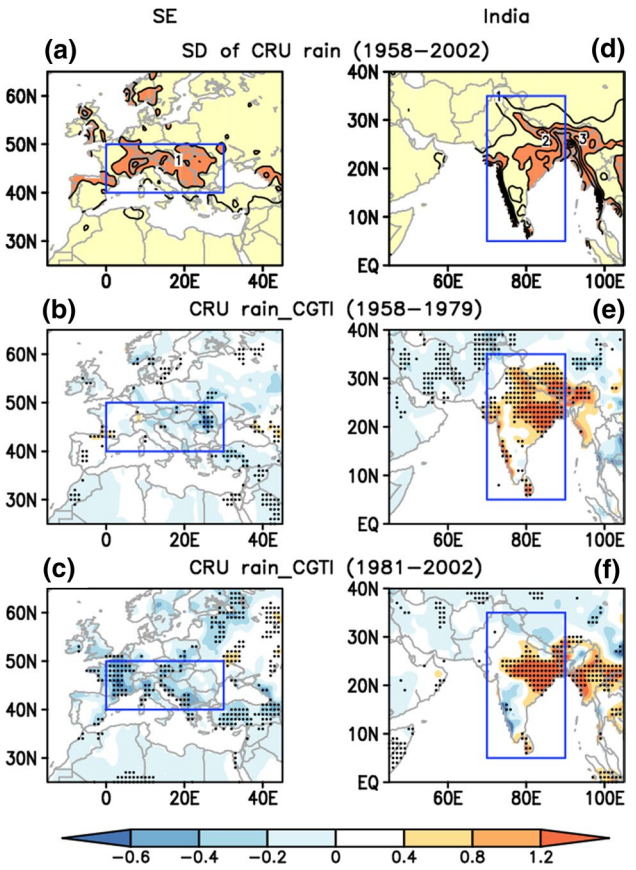

Fig. 4 **a**, **d** Interannual standard deviation (SD) of rainfall in June during 1958–2002 over **a** SE and **d** India. *Shading* depicts the region with SD exceeding 1 mm d^{-1} in (**a**) and 2 mm d^{-1} in (**d**) and contour interval is 0.5 mm d^{-1} in (**a**) and 1 mm d^{-1} in (**d**). **b**–**f** Anomalies of CRU precipitation (*shading*) regressed against the CGTI during **b**, **e** 1958–1979 and **c**, **f** 1981–2002 over SE (**b**, **c**) and India (**e**, **f**).Regions with significant precipitation anomalies are *dotted*. The *blue rectangle* depicts the SE region (40°–50°N, 0°–30°E) in (**a**–**c**) and India (5°–35°N, 70°–90°E) in (**d**–**f**)

similar result is obtained, with the correlation coefficients of −0.41 between the CGTI and the SERI during the second epoch and −0.22 during the first epoch (Table 1). The relationship in early summer between the CGT and the SE rainfall is enhanced after the late 1970s.

The enhanced impact of the SE rainfall on the CGT after the late 1970s is indicated by the H200 anomalies related to the negative SERI (Fig. 6). Here sign is flipped for the SERI to facilitate its comparison with the circulation anomalies related to the CGTI (Fig. 1). The SE rainfall during the pre-1980 epoch is only associated with an upstream wave train propagating southeastward from eastern North Atlantic into SE (Fig. 6a), indicating a link of the SE rainfall to the upstream disturbance. During the post-1980 epoch, both mid-latitude and high-latitude wave trains are seen in the downstream of the rainfall anomalies over SE (Fig. 6b), which resembles those related to the CGTI

Table 1 Correlation coefficient of the CGTI with the Indian rainfall index (IRI) and the SE rainfall index (SERI) during 1958–1979 and 1981–2002 based on the CRU precipitation data

	IRI	SERI
1958–1979	0.84* (0.64*)	–0.16 (–0.22)
1981–2002	0.60* (0.55*)	–0.53* (–0.41)

Values in the parentheses are based on the NOAA precipitation data

* Significant at the confidence level of 95 %

(Fig. 1b), suggesting a probable role of the rainfall over SE in the CGT.

In addition, Ding and Wang (2005) proposed that the Indian summer monsoon rainfall can induce formation of the CGT pattern. In early summer, rainfall exhibits strong interannual variability over Indian subcontinent with the maximum in northeast India exceeding 2 mm per day (Fig. 4d), twice that over SE (Fig. 4a). To explore whether the Indian summer monsoon rainfall also contributes to the spatial pattern change of the early-summer CGT identified in Sect. 3, rainfall anomalies over the Indian subcontinent related to the CGTI during the pre- and post-1980 epochs are shown in Fig. 4e, f. In the positive phase of the CGT pattern, rainfall increases significantly in India during both epochs. The correlation coefficients between the CGTI and the Indian rainfall index (IRI), which is defined as mean rainfall in June averaged over the region (5°–35°N, 70°–90°E) depicted by the blue rectangle in Fig. 4d, f, are 0.84 (0.60) based on the CRU rainfall data and 0.64 (0.55) based on the NOAA rainfall data during the pre- (post-) 1980 epoch (Table 1), respectively.

The Indian rainfall is linked to a mid-latitude wave train along the westerly jet circling the whole Northern Hemisphere during the pre-1980 epoch (Fig. 7a). A similar wave train is also identified in relation to the Indian rainfall during the post-1980 epoch (Fig. 7b). Note that the magnitude of the positive anomalies of H200 over west-central Asia is weaker during the second epoch than that during the first epoch, which is consistent with the weakened relation of the CGT with the Indian rainfall (Table 1). Additionally, a high-latitude wave train over northern Eurasia is also observed during the second epoch. The spatial pattern change related to the Indian rainfall, from a mid-latitude wave train during the first epoch to two mid- and high-latitude wave trains during the second epoch, is similar to that related to the CGTI (Fig. 1). The similarity suggests that the CGT pattern

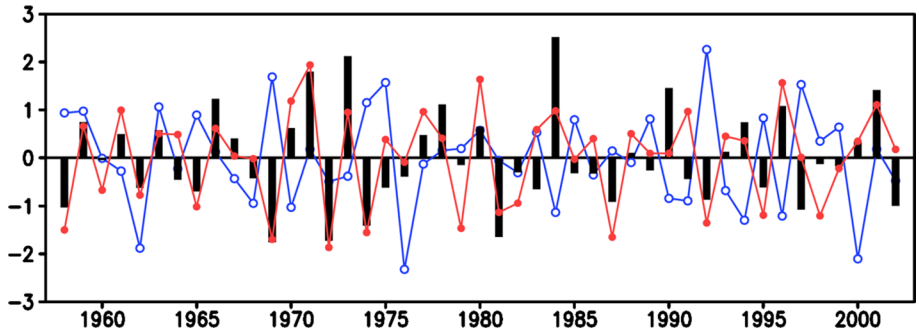

Fig. 5 Time series of the CGTI (*bar*), the SERI (*blue line with empty circle*), and the IRI (*red line with filled circle*). See text for details of the definition of the three indices

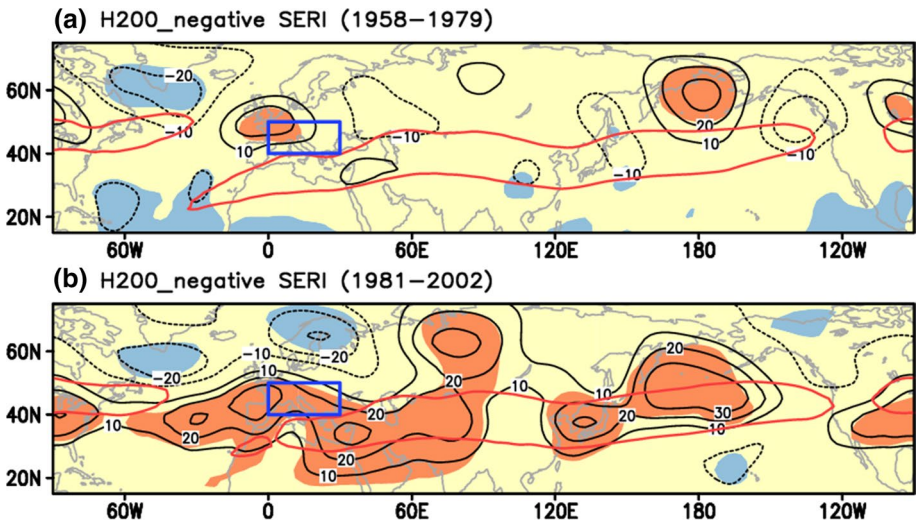

Fig. 6 As in Fig. 1, but for H200 anomalies regressed against the negative SERI. *The blue box* depicts the SE region

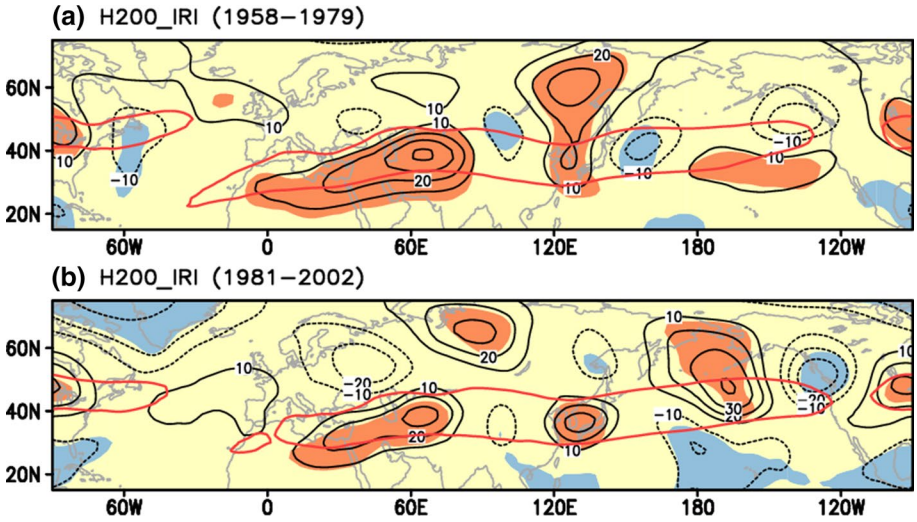

Fig. 7 As in Fig. 1, but for H200 anomalies regressed against the IRI

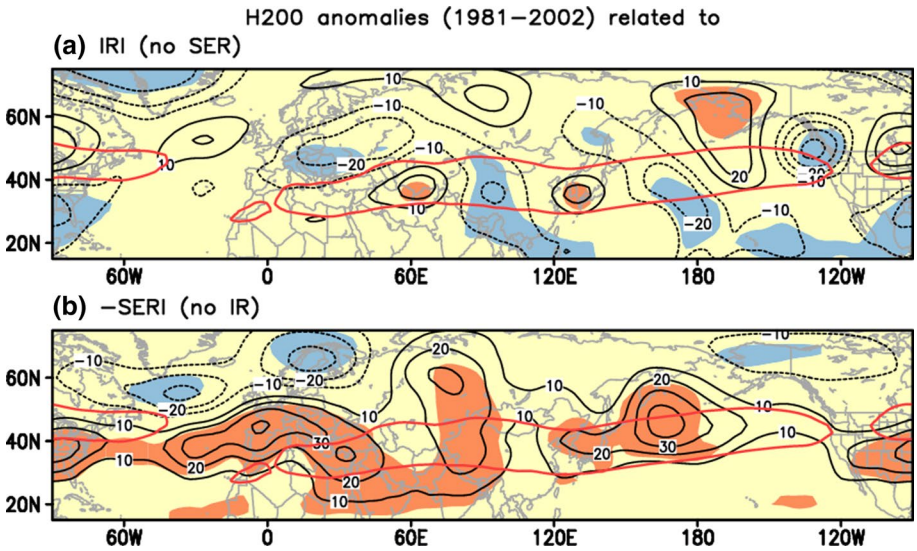

Fig. 8 As in Fig. 1b, but for H200 anomalies regressed against the IRI after removing the effect of the SE rainfall (**a**) and against the negative SERI after removing the effect of the Indian rainfall (**b**) during 1981–2002. The effect of the SE and Indian rainfall is removed by subtracting the component linearly regressed upon the SERI and IRI, respectively

change identified in Sect. 3 is also related to the Indian rainfall, in addition to the SE rainfall.

Meanwhile, the rainfalls over the two regions (SE and India) are significantly correlated during the post-1980 epoch, with a correlation coefficient of −0.42 between the SERI and IRI, but not during the pre-1980 epoch with a correlation coefficient of −0.2. Consequently, during the post-1980 epoch, the H200 anomalies related to the Indian rainfall (Fig. 7b) may include the effect of the SE rainfall and the H200 anomalies related to the SE rainfall (Fig. 6b) may include the effect of the Indian rainfall. To further explore effect of the rainfall in SE and India independently, partial regressed results during the post-1980 epoch are presented in Fig. 8. The partial regressed results with regard to the IRI are obtained by regressing H200 anomalies against the IRI after removing the effect of the SE rainfall (Fig. 8a). Likewise the partial regression with regard to the SERI is obtained by regressing H200 anomalies against the negative SERI after removing the effect of the Indian rainfall (Fig. 8b). Specifically, the effect of the SE and Indian rainfall is removed by subtracting the component linearly regressed upon the SERI and IRI, respectively. Related to the IRI, the significant signals of the high-latitude wave train basically disappear after the effect of the SE rainfall is removed (Fig. 8a). Meanwhile, the intensity of the mid-latitude wave train is also reduced. On the other hand, after removing the effect of the Indian rainfall, both the mid- and high-latitude wave trains related to the SE rainfall (Fig. 8b) maintain a similar spatial pattern to that post-1980 as before (Fig. 6b). The results indicate that during the post-1980 epoch the mid-latitude wave train of the CGT is associated with both rainfall anomalies over India and SE, and the high-latitude wave train is, however, more directly associated with the rainfall anomalies over SE. Note that related to the SE rainfall, the mid-latitude wave train pattern over southwest Asia is displaced from the CGT pattern (Fig. 1b)

by roughly one quarter of wavelength. We also calculate the independent effect of the rainfall in Indian and SE during the pre-1980 epoch using the same partially-regressed method (figures not shown). The result is similar to that in Figs. 6a, 7a: The Indian rainfall is related to the mid-latitude wave train along the strong upper-troposphere jet and the SE rainfall is associated with the upstream anomalies over the North Atlantic.

Wang et al. (2012) also found a significant change in the summer-mean CGT, specifically over the North Atlantic–Europe sector, around the late 1970s. They postulated that this change is mostly attributed to the enhanced impact of the west African monsoon rainfall. We have examined the relationship between the CGT change and west African rainfall anomalies in early summer. The CGT is significantly linked to rainfall anomalies in the subtropical (10°–15°N) west African land before the late 1970s, while their relation becomes weak after the late 1970s (figures not shown). The weakened relationship suggests that the subtropical west African rainfall is not the driver of the early-summer CGT pattern change after the late 1970s. This hypothesis is confirmed by the circulation anomalies related to the subtropical west African rainfall, with no significant high-latitude signals over northern Eurasia after the late 1970s (figure not shown).

In summary, the observational results show that during the post-1980 epoch the CGT pattern is related to rainfall anomalies in India and SE. Both rainfalls contribute to formation of the mid-latitude wave train of the CGT pattern, but the high-latitude wave train of the CGT pattern is more directly tied to the SE rainfall anomalies than Indian rainfall anomalies. The coupled SE and Indian rainfall together induces the two wave-train pattern of CGT after the late 1970s. During the pre-1980 epoch, the CGT is mostly contributed to by the rainfall anomalies in India, which is decoupled from the rainfall anomalies in SE. The results lead to a conclusion that the SE rainfall reshapes the spatial pattern of the early-summer CGT after the late 1970s. In the next subsection, the conclusion is further investigated using the LBM that is briefly introduced in Sect. 2.

4.2 LBM results

Two heat forcings over SE and India are prescribed in the LBM (Fig. 9e), to investigate impact of the rainfall anomalies in SE and India on the CGT. In the horizontal the heat forcing has a cosine squared profile in an elliptical region. The maximum heat forcing is -1.5 K per day over SE and 3 K per day over India, which is set to be at approximately 500 hPa ($\sigma = 0.45$) in the vertical. It corresponds to the regional-mean heat forcing of -0.5 K per day over SE and 1 K per day over India, half of the interannual standard deviation of diabatic heat about 1 K per day over SE and 2 K per day over India calculated as a residue of the thermodynamic equation (figure not shown).

Figure 9a shows the steady response of upper-tropospheric geopotential height anomalies to the prescribed heat sink over SE based on the basic flow in June for the period 1981–2002. The SE heat sink excites two wave trains. One wave train is trapped within the strong Asian westerly jet in mid latitudes of the Eurasian continent, with two positive centers over west Asia and East Asia. The other wave train is distributed in high latitudes over the northern Eurasia, with two negative centers over eastern Europe and eastern Siberia and one positive center in between over northern central Siberia. The two wave-train structure over Eurasia resembles that related to the CGT (Fig. 1b) and the negative SE rainfall (Figs. 6b, 8b) during the post-1980 epoch in the observation. The LBM result supports the conclusion based on the observational evidences that the SE heat sink reshapes the spatial pattern of the CGT after the late 1970s, inducing the high-latitude wave train of the CGT over northern Eurasia.

The Indian heat source, however, only induces a mid-latitude wave train within the strong Asian westerly jet (Fig. 9b) during the post-1980 epoch. Over the Eurasian continent the wave train features two positive centers over southwest Asia and east Asia in the upper troposphere, though the center shift westward roughly one quarter of wavelength over east Asia compared with that in the observation (Figs. 7b, 8a). In addition, the wave train also extends downstream into the North Pacific with reduced magnitude. The simulation result is in agreement with the observational H200 anomalies related to the Indian rainfall after removing the effect of the SE rainfall (Fig. 8a). In response to the combination of the Indian heat source and the SE heat sink, both high-latitude and mid-latitude wave trains of the CGT pattern are more clear (Fig. 9c), similar to the observational CGT pattern during the post-1980 epoch (Fig. 1b). The LBM results confirms the conclusion that the coupled Indian and SE heat forcing jointly induce the two wave-train pattern of the CGT during the post-1980 epoch, in which the Indian forcing contributes to the mid-latitude wave train and the SE forcing contributes to both the mid-latitude and high-latitude wave trains.

The response to the Indian heat source based on the basic state in June for the period 1958–1979 is also simulated in the LBM (Fig. 9d). A mid-latitude wave train along the Asian westerly jet is seen, resembling the observational H200 anomalies related to the Indian rainfall during the pre-1980 epoch (Fig. 7a). We conclude that the Indian rainfall causes the CGT pattern before the late 1970s.

Saeed et al. (2011b) introduced additional heating over the Indian monsoon heat low region during summer season

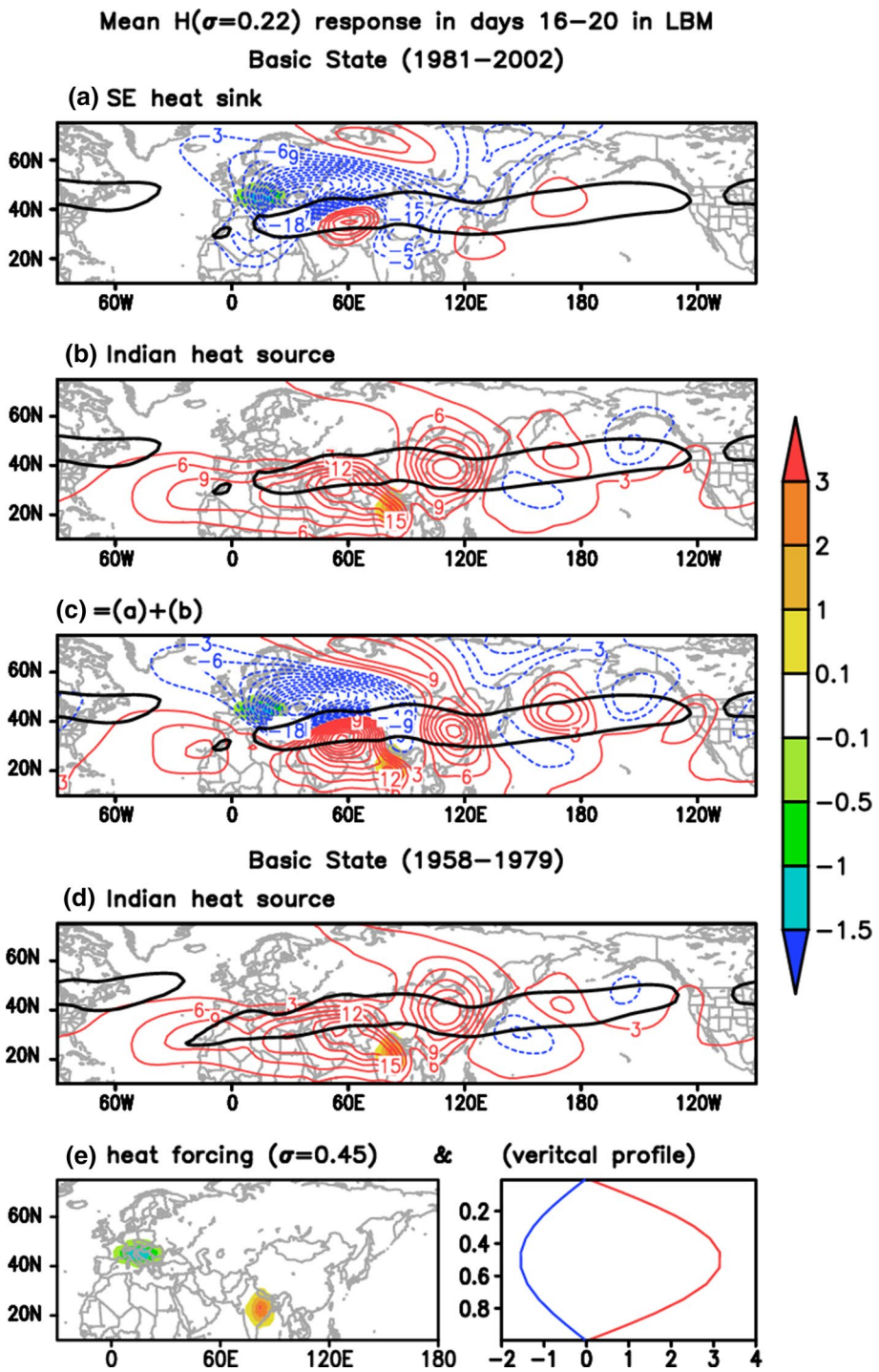

Fig. 9 **a**–**c** Mean geopotential height anomalies averaged for days 16–20 at the sigma level of 0.22 responded to **a** the SE heat sink, **b** the Indian heat source, and **c** their combination based on the June basic flow during 1981–2002 in the LBM. **d** As in (**b**), but based on the June basic flow during 1958–1979. **e** The *horizontal* distribution of the heat forcing at the sigma level of 0.45 (*left panel*) and vertical profile of the maxima at (22.5°N, 82.5°E) (*red line*) and of the minima at (45°N, 15°E) (blue line) in the sigma coordinate (*right panel*) with unit of K d^{-1} prescribed in the LBM. Shading depicts the prescribed forcing (K d^{-1}) and contour interval is 3 gpm. The *thick black contour* depicts the strong westerly jet exceeding 20 m s^{-1} in the basic flow

by modifying the local surface albedo in a global atmospheric general circulation model (AGCM). The response below the latitude of 60°N in the upper troposphere depicts two anticyclonic anomalies centered over west-central Asia and east Asia and two cyclonic anomalies in between and over European region, respectively (Saeed et al. 2011b, in their Fig. 1c). The cyclonic anomaly over the European region differs from the steady response to the Indian heat forcing in the LBM in the present study (Fig. 9b, d) and resembles that due to the combined effect of the SE and India heat forcing (Fig. 9c). One possible reason for the different response to the Indian heat forcing between the LBM and the AGCM could be because the AGCM takes into account the mid-latitude precipitation induced by the change in surface albedo over the Indian monsoon heat low region.

4.3 Discussion

4.3.1 Coupling of Indian and SE rainfall after the late 1970s

The observational evidence and simulation results with the LBM highlight the important role of coupling/decoupling of the Indian rainfall with the SE rainfall in the early-summer CGT pattern change. When the Indian rainfall is coupled with the SE rainfall after the late 1970s, both rainfalls together induce a two wave-train pattern of CGT (Figs. 1b, 7b, 9c). In contrary, before the late 1970s when the Indian rainfall is decoupled from the SE rainfall, the Indian rainfall only triggers a mid-latitude wave train of CGT (Figs. 1a, 7a, 9d). Why did the SE and Indian rainfall couple together after the late 1970s, but not before the late 1970s?

The coupling is probably due to the mid-latitude circumglobal wave train of the CGT induced by the Indian rainfall (Fig. 7). Ding and Wang (2005) proposed that the Indian rainfall can trigger a mid-latitude wave train with a zonal wavenumber of five along the upper-tropospheric subtropical westerly jet in the Northern Hemisphere. The five centers with positive H200 anomalies are located over southwest Asia, east Asia, central North Pacific, North America, and western Europe in early summer (Fig. 7). Specifically, the anticyclonic anomaly over western Europe is formed to the west of the British Island (50°–60°N) during the pre-1980 epoch (Fig. 7a), north of that to the west of SE (40°–50°N) during the post-1980 epoch (Fig. 7b). A lower-tropospheric northerly anomaly in the east of the barotropic anticyclonic anomaly (Fig. 10b), although insignificant, suppresses northward moisture transport and, subsequently, rainfall over SE during the post-1980 epoch, leading to significant coupling between Indian and SE rainfall. The northerly anomaly during the pre-1980 epoch, however, prevails to the north of 50°N over the high-latitude North Atlantic (Fig. 10a), exerting a negligible role in SE rainfall that is consistent with the decoupling of the SE rainfall from Indian rainfall before the late 1970s. The northward displacement of the anticyclonic anomaly over western Europe during the first epoch is possibly related to change in the basic flow over the North Atlantic: The westerly jet extends northeastward during the first epoch (Fig. 7a) and eastward during the second epoch (Fig. 7b). Subsequently, the CGT wave train trapped with the North Atlantic westerly jet propagates northeastward during the first epoch (Fig. 7a) and develops eastward during the second epoch (Fig. 7b), leading to the northward located anticyclonic anomaly over western Europe during the first epoch.

In addition, the reduced SE rainfall may also feedback the CGT and Indian rainfall, enhancing the coupling of the SE and Indian rainfall after the late 1970s. The SE heat

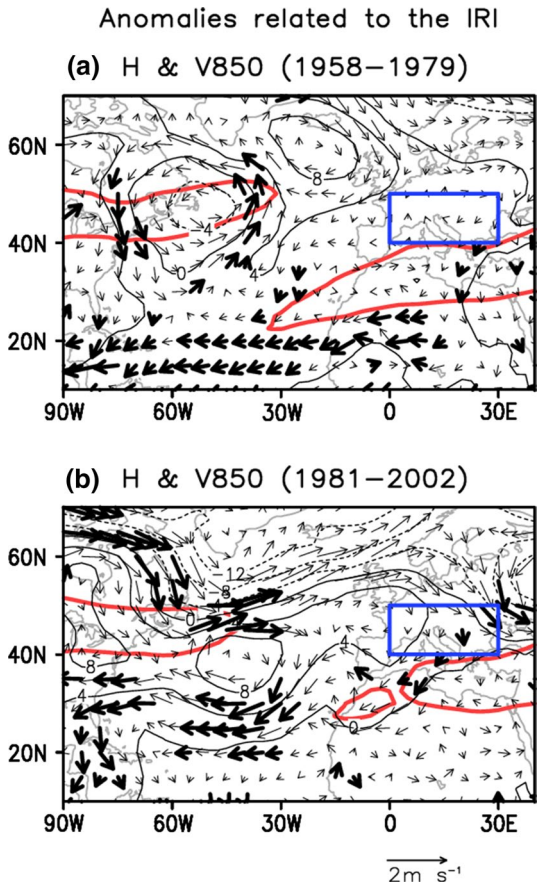

Fig. 10 As in Fig. 7, but for regressed anomalies of geopotential height (contour) and *horizontal winds* (vector) at 850 hPa. Contour interval is 4 gpm. *Black thick vectors* are where zonal or meridional wind is significant at the 95 % confidence level and the *red thick contour* depicts the strong westerly jet exceeding 20 m s^{-1} at 200 hPa. The *blue rectangle* depicts the SE region

sink can induce a downstream wave train along the Asian westerly jet, with a positive H200 anomaly over west Asia (Figs. 8b, 9a). The positive anomaly increases meridional gradient between the Eurasian land and the Indian Ocean sea and, subsequently, enhances the Asian summer monsoon and rainfall in India (Ding and Wang 2005; Saeed et al. 2011a; Syed et al. 2012). The precise mechanism linking Indian and SE rainfall invites further studies.

4.3.2 Rainfall-circulation interaction over SE

The interannual reduction of rainfall over SE is associated with a local anticyclonic anomaly to the west during the pre- and post-1980 epochs in the upper troposphere (Fig. 6). The northerly anomaly in the east of the barotropic anticyclonic anomaly suppresses moisture transports towards SE and reduces local rainfall (figure not shown). Accordingly, the anticyclonic anomaly to the west of SE induced by the Indian rainfall after the late 1970s (Figs. 7b,

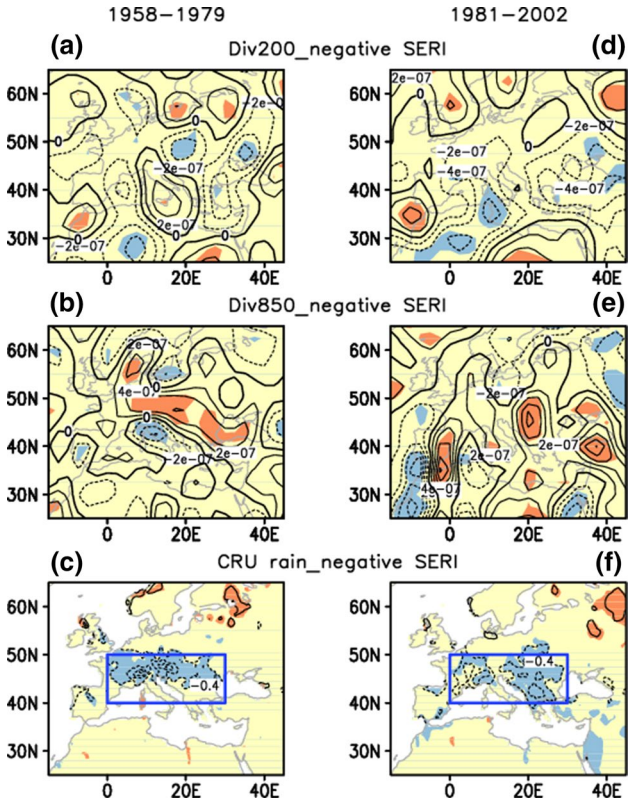

Fig. 11 Anomalies of horizontal divergence at **a**, **d** 200 hPa and **b**, **e** 850 hPa, and **c**, **f** CRU precipitation regressed against the negative SERI during **a**–**c** 1958–1979 and **d**–**f** 1981–2002. Shading indicates significance at the 95 % confidence level and contour interval is 2×10^{-7} s^{-1} for divergence (**a**–**e**) and 0.4 mm d^{-1} for precipitation (**c**, **f**). The *blue rectangle* depicts the SE region in (**c**, **f**)

10b) leads to reduced rainfall over SE as discussed in the last Sect. 4.3.1.

The SE rainfall could feed back to circulation during the post-1980 epoch (Fig. 6b). The feedback of SE rainfall is also supported by the LBM model simulation. With a prescribed SE heat sink, the LBM simulates two downstream wave trains during the post-1980 epoch (Fig. 9a). But why in the pre-1980 epoch the SE rainfall did not excite the CGT pattern (Fig. 6a)? We have examined standard deviation of rainfall over SE during the pre- and post-1980 epochs and found no significant change in its magnitude (figure not shown). In addition, the steady response to the SE heat sink is not sensitive to the basic state change over Eurasia between the pre- and post-1980 epochs, which is explored in the next subsection.

The feedback of the SE rainfall may relate to interaction of the SE rainfall with local divergence circulation (Fig. 11). During the post-1980 epoch, the reduced SE rainfall is associated with consistent convergence anomalies in the upper troposphere over SE (Fig. 11d) and divergence anomalies in the lower troposphere (Fig. 11e). However, the convergence/divergence signals related to the SE rainfall during the pre-1980 epoch (Fig. 11a, b) are regional-dependent, especially in the upper troposphere (Fig. 11a). The correlation coefficients are −0.38 (−0.61) between the negative SERI and the horizontal divergence at 200 hPa averaged over the SE region during the first (second) epoch. Accordingly, the local coupling of the upper-tropospheric convergence with reduced rainfall over SE is enhanced during the post-1980 epoch. The uniform upper-tropospheric convergence anomalies related to the negative SERI (Fig. 11d), acting as a Rossby wave source (Sardeshmukh and Hoskins 1988), excites a CGT-like pattern in the downstream Eurasian region (Figs. 8b, 9a). In the pre-1980 epoch, the regional-mean upper-tropospheric convergence (Fig. 11a) is weak and, therefore, limits circulation response to the SE rainfall during the pre-1980 epoch. However, more details on rainfall-circulation interaction over the SE region need a more complicated AGCM, which includes cloud-precipitation parameterization.

4.3.3 *Effect of basic flow on two wave train pattern of the CGT*

The present study revealed two mid- and high-latitude wave trains of the CGT over Eurasia after the late 1970s in early summer (Fig. 1b). A similar two–wave train pattern was found related to a precipitation see-saw pattern between Northeast Asia and Siberia in summer (Iwao and Takahashi 2008). In addition, a high-latitude wave-like teleconnection pattern was also identified related to formation of the Okhotsk high (Nakamura and Fukamachi 2004; Wakabayashi and Kawamura 2004). Iwao and Takahashi (2008) proposed that the zonal propagation of wave flux in mid-latitude is due to the waveguide effect of the strong Asian subtropical westerly jet and that in high-latitude due to the polar front jet. The two waveguides are also identified in early summer during the post-1980 epoch (Fig. 12). The spatial distribution of the stationary Rossby wavenumber (Hoskins and Ambrizzi 1993) of the 200-hPa basic flow exhibits two maxima in the Northern Hemisphere. It depicts two waveguides in mid-latitude around 40°N and in high-latitude at 60°N, respectively, in agreement with the location of the two wave trains of the CGT after the late 1970s (Fig. 1b). The two waveguides, therefore, provide favorable condition for formation of the two wave trains of CGT during the post-1980 epoch. On the other hand, two waveguides are also revealed during the pre-1980 epoch (figure not shown), similar to that during the post-1980 epoch (Fig. 12). The absence of the high-latitude wave train of the CGT during the first epoch suggests that the role of the basic flow change over Eurasia around the late 1970s in the CGT pattern change is secondary. The conclusion is also confirmed by the LBM simulation results. As the SE

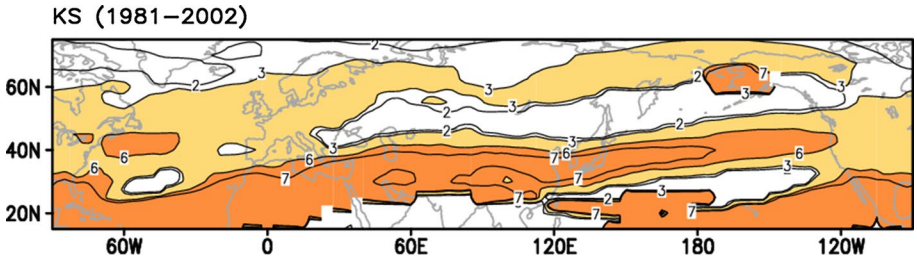

Fig. 12 Stationary Rossby wavenumber (KS) of the June basic flow at 200 hPa during 1981–2002. *Yellow* and *orange shading* depict region with KS exceeding 3 and 6, respectively

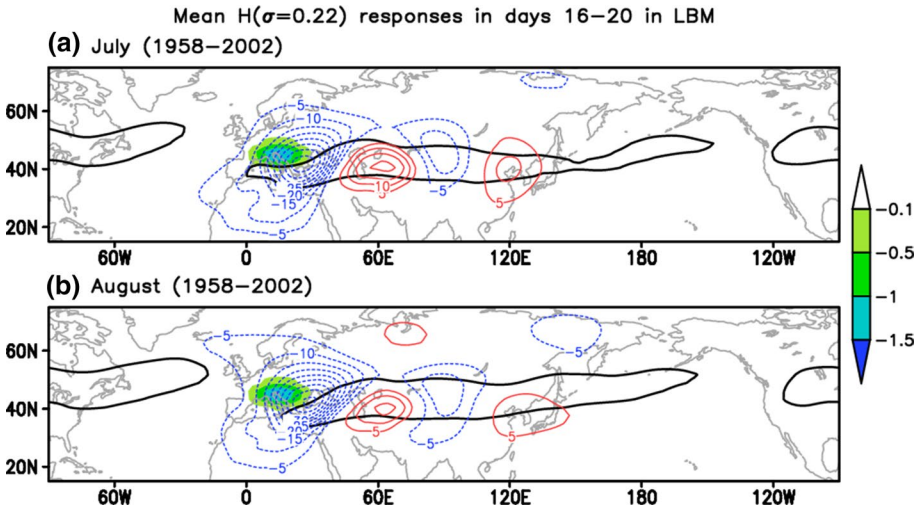

Fig. 13 As in Fig. 9a, but based on the basic flow in July (**a**) and August (**b**) during 1958–2002

heat sink is prescribed in the LBM, the two wave trains are also excited based on basic flow during the pre-1980 epoch (figure not shown), similar to that during the post-1980 epoch (Fig. 9a). Meanwhile, without effect of the SE rainfall, the Indian rainfall only induces a mid-latitude wave train of the CGT based on both the basic flow for the period 1958–1979 (Fig. 9d) and 1981–2002 (Fig. 9b).

5 July and August situations

The discussion so far has focused on the decadal change of the CGT in June. What happened to the CGT in July and August? It is found that related to the CGTI, no significant high-latitude wave train over northern Eurasia is evident (figures not shown), albeit strong interannual standard deviation of 1 mm per day occurred over SE in July and August as the case in June. The absence of the high-latitude wave train of the CGT in July and August was also revealed by Ding and Wang (2005, in their Fig. 5b, c) based on the NCEP/NCAR reanalysis data for the period 1948–2003. Why does the SE rainfall in July and August fail to stimulate a similar two wave trains as in June?

One possibility is that the mean state in July–August does not favor generation of northern branch of wave train. Numerical experiments with the LBM are carried out to test this idea. Figure 13 shows the response of the geopotential height anomalies to the SE heat sink based on the basic flow during 1958–2002 in July (Fig. 13a) and August (Fig. 13b). The responses are mainly trapped within the strong westerly jet over mid-latitude Eurasia in both July and August. There are only patchy signals in high latitudes over northern Eurasian continent, which are much weaker than the counterpart in the mid latitudes. Similar responses are obtained based on the basic flow during

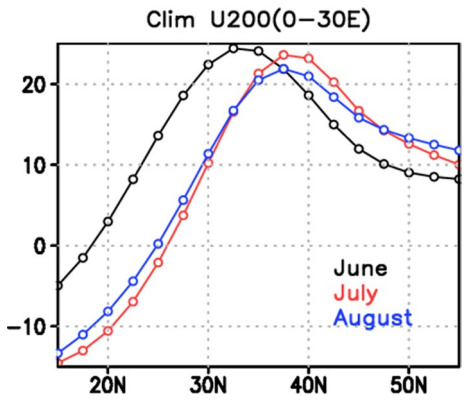

Fig. 14 Climatological zonal-mean zonal wind at 200 hPa averaged over 0°–30°E in June (*black line*), July (*red line*), and August (*blue line*) during 1958–2002

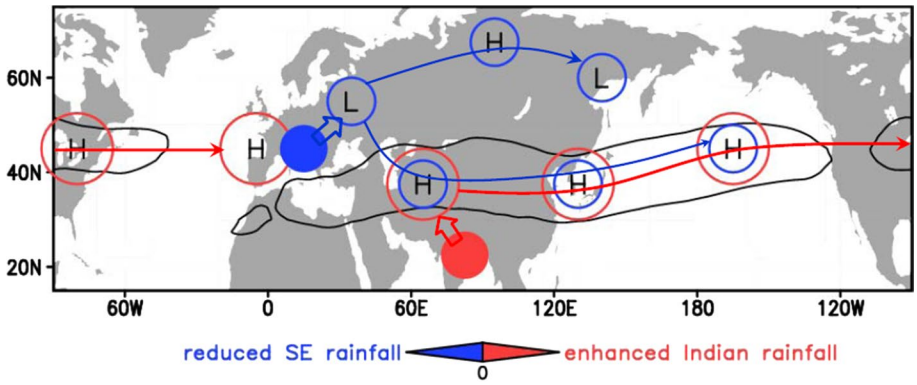

Fig. 15 Schematic diagram illustrating mechanism of the CGT in early summer. The *red circles* reflect effect of the enhanced Indian rainfall and the blue circles depict effect of the reduced SE rainfall

both the pre- and post-1980 epochs. The different circulation responses to the SE heat sink in June versus in July and August are likely attributed to the northward seasonal March of the strong westerly jet. Over the SE region, the westerly jet core advances northward from 32.5°N in June to 37.5°N in July and August (Fig. 14). Consequently, the SE heat sink is located in the entrance of the strong Asian westerly jet in July and August so that the responses are trapped within the downstream westerly jet due to its waveguide effect (Hoskins and Ambrizzi 1993).

6 Conclusion

A significant decadal change of the early-summer CGT is identified around the late 1970s. The CGT wave train along the strong upper-tropospheric westerly jet in mid latitudes of Northern Hemisphere dominated during the pre-1980 epoch has remained in the post-1980 epoch; however, a big change in the CGT pattern is the occurrence of another wave train in the high latitudes over northern Eurasia during the second epoch. The high-latitude wave train originates over eastern Europe and extends northeastward through central Siberia into Far East along a great circle route.

The change in the early-summer CGT pattern during the post-1980 epoch is caused by rainfall anomalies over SE. Figure 15 summarized mechanisms for the formation of CGT pattern in early summer. The mid-latitude wave train of the CGT is mainly caused by Indian rainfall anomalies and partially by the SE rainfall anomalies, whereas the high-latitude wave train of the CGT is primarily induced by the SE rainfall anomalies. The coupled Indian and SE rainfall together lead to the two wave-train pattern of CGT after the late 1970s.

Acknowledgments We thank three reviewers and the editor for their valuable comments, which greatly improved the manuscript. Research was supported by the National Natural Science Foundation of China (Grant Nos. 41375086 and 41320104007).

References

Ambrizzi T, Hoskins BJ, Hsu HH (1995) Rossby wave propagation and teleconnection patterns in the Austral winter. J Atmos Sci 52:3661–3672

Chen G, Huang R (2012) Excitation mechanisms of the teleconnection patterns affecting the July precipitation in Northwest China. J Clim 25:7834–7851. doi:10.1175/jcli-d-11-00684.1

Chen M, Xie P, Janowiak JE, Arkin PA (2002) Global land precipitation: a 50-yr monthly analysis based on gauge observations. J Hydrometeorol 3:249–266

Chen G, Huang R, Zhou L (2013) Baroclinic instability of the silk road pattern induced by thermal damping. J Atmos Sci 70:2875–2893. doi:10.1175/jas-d-12-0326.1

Ding Q, Wang B (2005) Circumglobal teleconnection in the Northern Hemisphere summer. J Clim 18:3483–3505

Ding Q, Wang B, Wallace JM, Branstator G (2011) Tropical-extratropical teleconnections in boreal summer: observed interannual variability. J Clim 24:1878–1896. doi:10.1175/2011jcli3621.1

Enomoto T (2004) Interannual variability of the Bonin high associated with the propagation of Rossby waves along the Asian jet. J Meteorol Soc Jpn 82:1019–1034

Enomoto T, Hoskins BJ, Matsuda Y (2003) The formation mechanism of the Bonin high in August. Q J R Meteorol Soc 129:157–178. doi:10.1256/qj.01.211

Fisher RA (1921) On the 'probable error' of a coefficient of correlation deduced from a small sample. Metron 1:3–32

Hoskins BJ, Ambrizzi T (1993) Rossby wave propagation on a realistic longitudinally varying flow. J Atmos Sci 50:1661–1671

Hoskins BJ, Karoly DJ (1981) The steady linear response of a spherical atmosphere to thermal and orographic forcing. J Atmos Sci 38:1179–1196

Huang G, Liu Y, Huang R (2011) The interannual variability of summer rainfall in the arid and semiarid regions of Northern China and its association with the Northern Hemisphere circumglobal teleconnection. Adv Atmos Sci 28:257–268. doi:10.1007/s00376-010-9225-x

Huang W, Feng S, Chen J, Chen F (2015) Physical mechanisms of summer precipitation variations in the Tarim basin in northwestern China. J Clim 28:3579–3591. doi:10.1175/jcli-d-14-00395.1

Iwao K, Takahashi M (2008) A precipitation seesaw mode between Northeast Asia and Siberia in summer caused by Rossby waves over the Eurasian continent. J Clim 21:2401–2419. doi:10.1175/2007JCLI1949.1

Kalnay E, Kanamitsu M, Kistler R, Collins W, Deaven D, Gandin L, Iredell M, Saha S, White G, Woollen J (1996) The NCEP/NCAR 40-year reanalysis project. Bull Am Meteorol Soc 77:437–471

Kosaka Y, Nakamura H, Watanabe M, Kimoto M (2009) Analysis on the dynamics of a wave-like teleconnection pattern along the

summertime Asian jet based on a reanalysis dataset and climate model simulations. J Meteorol Soc Jpn 87:561–580

Lau K-M, Weng H-Y (2002) Recurrent teleconnection patterns linking summertime precipitation variability over east Asia and North America. J Meteorol Soc Jpn 80:1309–1324

Li C, Wu L, Chang P (2010) A far-reaching footprint of the tropical Pacific meridional mode on the summer rainfall over the Yellow River loop valley. J Clim 24:2585–2598. doi:10.1175/2010jcli3844.1

Lin H (2009) Global extratropical response to diabatic heating variability of the Asian summer monsoon. J Atmos Sci 66:2697–2713. doi:10.1175/2009jas3008.1

Lin Z (2014) Intercomparison of impacts of four summer teleconnections over Eurasia on East Asian rainfall. Adv Atmos Sci 31:1366–1376. doi:10.1007/s00376-014-3171-y

Lin Z, Lu R (2016) Impact of summer rainfall over southern-central Europe on circumglobal teleconnection. Atmos Sci Lett 17:258–262. doi:10.1002/asl.652

Liu F, Wang B (2013) Mechanisms of global teleconnections associated with the Asian summer monsoon: an intermediate model analysis. J Clim 26:1791–1806

Lu R-Y, Oh J-H, Kim B-J (2002) A teleconnection pattern in upper-level meridional wind over the North African and Eurasian continent in summer. Tellus A 54:44–55

Mitchell TD, Jones PD (2005) An improved method of constructing a database of monthly climate observations and associated high-resolution grids. Int J Climatol 25:693–712. doi:10.1002/joc.1181

Nakamura H, Fukamachi T (2004) Evolution and dynamics of summertime blocking over the Far East and the associated surface Okhotsk high. Q J R Meteorol Soc 130:1213–1233. doi:10.1256/qj.03.101

Rodwell MJ, Hoskins BJ (1996) Monsoons and the dynamics of deserts. Q J R Meteorol Soc 122:1385–1404

Saeed S, Müller WA, Hagemann S, Jacob D (2011a) Circumglobal wave train and the summer monsoon over northwestern India and Pakistan: the explicit role of the surface heat low. Clim Dyn 37:1045–1060. doi:10.1007/s00382-010-0888-x

Saeed S, Müller WA, Hagemann S, Jacob D, Mujumdar M, Krishnan R (2011b) Precipitation variability over the South Asian monsoon heat low and associated teleconnections. Geophys Res Lett 38:L08702. doi:10.1029/2011GL046984

Saeed S, Lipzig N, Müller WA, Saeed F, Zanchettin D (2014) Influence of the circumglobal wave-train on European summer precipitation. Clim Dyn 43:503–515. doi:10.1007/s00382-013-1871-0

Sardeshmukh PD, Hoskins BJ (1988) The generation of global rotational flow by steady idealized tropical divergence. J Atmos Sci 45:1228–1251

Sato N, Takahashi M (2006) Dynamical processes related to the appearance of quasi-stationary waves on the subtropical jet in midsummer Northern Hemisphere. J Clim 19:1531–1544

Schubert S, Wang H, Suarez M (2011) Warm season subseasonal variability and climate extremes in the Northern Hemisphere: the role of stationary Rossby waves. J Clim 24:4773–4792

Soon W, Dutta K, Legates DR, Velasco V, Zhang W (2011) Variation in surface air temperature of China during the 20th century. J Atmos Terr Phys 73:2331–2344. doi:10.1016/j.jastp.2011.07.007

Sun J, Wang H (2012) Changes of the connection between the summer North Atlantic Oscillation and the East Asian summer rainfall. J Geophys Res 117:D08110. doi:10.1029/2012jd017482

Sun J, Wang H, Yuan W (2008) Decadal variations of the relationship between the summer North Atlantic Oscillation and middle East Asian air temperature. J Geophys Res 113:D15107. doi:10.1029/2007JD009626

Syed F, Yoo J, Körnich H, Kucharski F (2012) Extratropical influences on the inter-annual variability of South-Asian monsoon. Clim Dyn 38:1661–1674. doi:10.1007/s00382-011-1059-4

Takaya K, Nakamura H (2001) A formulation of a phase-independent wave-activity flux for stationary and migratory quasigeostrophic eddies on a zonally varying basic flow. J Atmos Sci 58:608–627

Uppala SM, Kållberg P, Simmons A, Andrae U, Bechtold V, Fiorino M, Gibson J, Haseler J, Hernandez A, Kelly G (2005) The ERA-40 re-analysis. Q J R Meteorol Soc 131:2961–3012

Wakabayashi S, Kawamura R (2004) Extraction of major teleconnection patterns possibly associated with the anomalous summer climate in Japan. J Meteorol Soc Jpn 82:1577–1588

Wang B, Wu R, Lau KM (2001) Interannual variability of the Asian summer monsoon: contrasts between the Indian and the western North Pacific-East Asian monsoons*. J Clim 14:4073–4090

Wang H, Wang B, Huang F, Ding Q, Lee J-Y (2012) Interdecadal change of the boreal summer circumglobal teleconnection (1958–2010). Geophys Res Lett 39:L12704. doi:10.1029/2012gl052371

Watanabe M, Kimoto M (2000) Atmosphere-ocean thermal coupling in the North Atlantic: a positive feedback. Q J R Meteorol Soc 126:3343–3369

Yasui S, Watanabe M (2010) Forcing processes of the summertime circumglobal teleconnection pattern in a dry AGCM. J Clim 23:2093–2114. doi:10.1175/2009jcli3323.1

Yim S-Y, Wang B, Liu J, Wu Z (2014) A comparison of regional monsoon variability using monsoon indices. Clim Dyn 43:1423–1437. doi:10.1007/s00382-013-1956-9

Yun K-S, Kim S-Y, Ha K-J, Watanabe M (2011) Effects of subseasonal basic state changes on Rossby wave propagation during northern summer. J Geophys Res 116:D24102. doi:10.1029/2011jd016258